Atomic packing of the inherent structure of simple liquids

H. W. Sheng* and E. Ma
Department of Materials Science and Engineering, Johns Hopkins University, Baltimore, Maryland 21218, USA
(Received 6 November 2003; published 23 June 2004)

We report a universal inherent packing structure underlying the simple liquids, the normalized distribution functions of which are independent of temperature and density. The inherent packing state, carrying the maximized configurational entropy, has intrinsic connections with the maximally random jammed state of hard spheres.

DOI: 10.1103/PhysRevE.69.062202 PACS number(s): 61.20.Ne, 05.20.Jj, 61.43.Bn

Whereas the physics of liquids can be comprehended with the theory of thermodynamics and hydrodynamics [1], finding a unifying *structural* description for liquids remains a grand challenge in science [2]. The complexity of a liquid arises from the immense configurational space that it can access, where an organizing principle, such as the well-defined periodicity for crystals, is absent. The internal atomic arrangements of a liquid change with time as well, sampling the energy landscape associated with the atomic configurations. The difficulty in characterizing the liquid structure can be mitigated by studying its inherent, or "frozen-in" structure [3], where the influence of the thermal motions is removed. The inherent structure (IS) is obtained by mapping the configurations onto the local minima of the potential energy surface [3]. The atomic packing of the IS is the subject of this paper.

For the glasses formed by quenching the liquid, a structural model is that of Bernal's of static random-close-packing (RCP) of hard spheres [4,5]. However, the RCP state and its density (packing fraction) is found heavily dependent on the packing or densification protocols [5]. Only very recently has a unique RCP structure been defined—the maximally random jammed (MRJ) state of hard spheres [6]. Also, the glasses usually differ in structure from their liquid precursors, due to, for example, the complex structural relaxation that occurs during the quench. A link between the liquid, or the atomic packing of its inherent structure, and the RCP is hitherto not established.

In this paper, we analyze the geometrical packing structure of the mechanically stable IS that underlies the liquid. The inherent packing (IP) uncovered will be correlated with the MRJ state. Standard molecular-dynamics (MD) simulation methods [7] and a monatomic Lennard-Jones system are employed, using canonical (*NVT*) ensembles with periodic boundary conditions. The truncated and shifted force field [8] was used with a cutoff distance $r_c = 2.5$. Reduced units are used: length in units of σ, temperature (T) in units of ε/k_B, and time in units of $\sqrt{\sigma^2 m/\varepsilon}$, where m is the mass of the particles. The time step is 0.0024. Temperature control was achieved by coupling the system with a Nose-Hoover thermostat.

In our simulations, IS is obtained by finding the local minima of the potential energy surface [3,9]. Energy minimization using the conjugate gradient method was performed on each instantaneous configuration without interrupting the dynamics of the system. The IS of the liquid system along an isochoric path is shown in Fig. 1. The energy landscape is observed to encompass three distinct regions: the equilibrium liquid at high temperatures, the supercooled liquid at intermediate temperatures, and the glassy state below the glass transition temperature.

Above a transition temperature T_A, the average IS energy (e_{IS}) is constant at all temperatures. The gradual change of e_{IS} at T_A signifies the onset of the slow dynamics, and the entrance into the supercooled region. In the supercooled re-

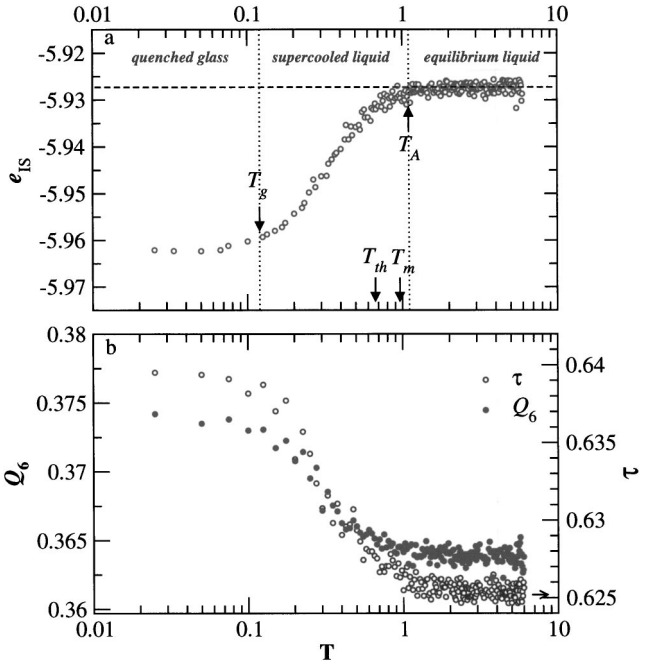

FIG. 1. (Color online) (a) The potential energy of the inherent structures (e_{IS}) of a Lennard-Jones monatomic system ($\rho = 0.9, 864$ particles) along an isochoric path (cooling rate = 0.01). The liquid freezes into the glass below $T_g = 0.12$. Each data point represents 200 configurations. For comparison, the actual melting temperature T_m and the thermodynamic melting temperature T_{th} of the corresponding LJ crystal are also shown [30]. (b) The change of the local bond-orientational order (Q_6) and the translational order parameter (τ) of the inherent structures during the quench. Each data point represents 50 configurations.

*Corresponding author. Electronic address: hwsheng@jhu.edu

gion, the liquid falls out of equilibrium, sampling deeper basins where structural relaxation is expected to set in. Glass transition eventually takes place when the temperature drops to $T=0.12$, when the system is trapped in the basin of attraction and the activation process dominates [9].

The liquid transitions demonstrated in the energy landscape paradigm can be ascribed to its structural changes, e.g., icosahedral ordering [10–12]. To better quantify the structural changes, we use two order parameters: the orientational and its conjugated translational order parameter [13–16]. Here we adopt the local bond-orientational order parameter [14], Q_6, which is found to be more sensitive and stable to the structural change than the global order parameter as originally proposed by Steinhardt *et al.* [10]. The Voronoi construction method [17] is used to precisely determine the local bonds of individual atoms. To evaluate the translational order parameter τ we calculate $\tau=(1/s_c)\int_0^{s_c}|g(s)-1|ds$ [15], where, $s=r\rho^{1/3}$ is the radial distance scaled by the number density, $g(s)$ is the pair correlation function, $s_c=3.5$ is a numerical cutoff. As shown in Fig. 1(b), both Q_6 and τ of the IS's change monotonically with T, consistent with the energy landscape picture. In the equilibrium liquid state, these order parameters are the smallest and independent of the initial states. By contrast, in the off-equilibrium state, the structural order develops progressively, as reflected from the increase of Q_6 and τ, until the final glassy state is attained.

An important implication of Fig. 1 is that the IS's of the equilibrium liquid have the same degree of order. This suggests a unique statistical arrangement of the atoms in the IS's. To shed light on the details of the atomic distributions, we preformed an in-depth geometrical statistical analysis on the system using the Voronoi tessellation method, shown in Fig. 2. The Voronoi polyhedra offer direct information about the coordination, size, and asphericity of individual atoms, through which, the nature of the atomic packing can be characterized. For the high-T liquids, the Voronoi cell volume distribution (defined in terms of its probability distribution function) changes with T, and can be best fitted by a three-parameter log-normal function,

$$P(v^*)=\frac{e^{[\ln(v^*-v^*_{\min})-\ln v^*_a]^2/2\sigma^2}}{\sqrt{2\pi(v^*-v^*_{\min})\sigma^2}},$$

where $v^*_{\min}$, v^*_a, and σ are fitting parameters. The universal distribution rule may explain why the liquids can be scaled onto one master curve, as shown by Starr *et al.* [18]. Similarly, the standard deviation σ_v scales with T as $\sigma_v \sim T^{0.25}$, reflecting the changes in the vibration properties of the particles as a function of T [18]. The high-T liquids exhibit nonsymmetric characteristics: with decreasing T, the mean value of the sphericity drops, in accord with the order parameter changes in Fig. 1(b). The inherent structures, in contrast, behave very differently: both the Voronoi cell volume distribution and the asphericity distribution fall upon the same master curves, irrespective of T, Fig. 2(b). This feature indicates an *identical* inherent packing (IP) of all the liquid structures, in terms of the statistical distributions. Other statistical metrics confirm this observation: the average number of faces and edges per face are also virtually identical for all

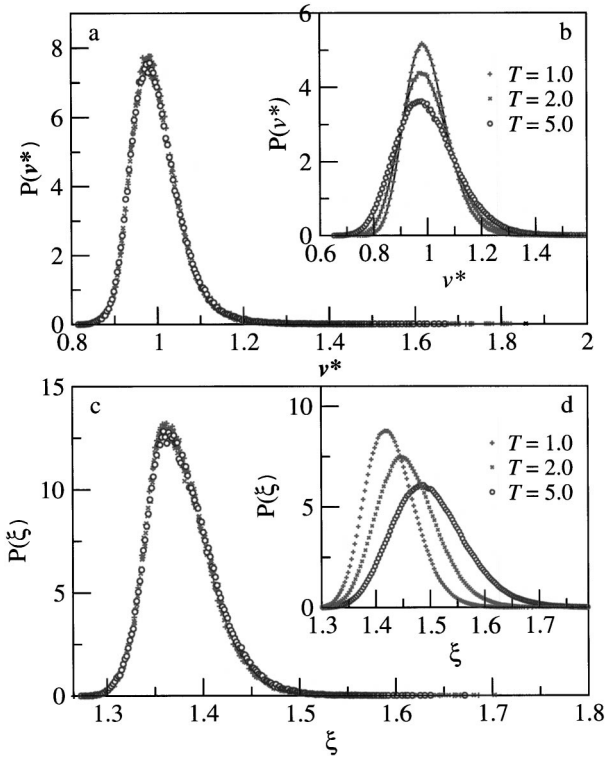

FIG. 2. (Color online) Geometrical statistics of the simple liquid ($T=1.0, 2.0, 5.0$, respectively) and the corresponding IS at $\rho=0.9$. The reduced volume v^* is defined as: $v^*=\rho v$. The volume probability distribution $P(v^*)$ is contrasted for (a) the inherent structures (b) the liquids at different temperatures, where the solid lines are the best fit of the probability distribution using the log-normal function. The asphericity [$\xi=(1/36\pi)(a^3/v^2)$, where a is the surface area of the Voronoi polyhedron, and v is its volume] probability distributions $P(\xi)$ are shown for (c) the inherent structures; and (d) the liquids at selected temperatures. Each line represents the average of 50 configurations of 10 976 particles.

$T>1.1$. Moreover, the IP of other studied densities (ranging from 0.8 to 1.2) showed the same geometrical statistics, indicating its universality.

On the contrary, configurations for the IS below T_A exhibit distribution profiles distinctly different from the IP of the equilibrium liquid. For the glasses ($T<T_g$), both the volume and the asphericity probability curves sharpen considerably (not shown), suggesting the localization of short-range ordering consistent with the decrease in energy (Fig. 1).

Naturally, one wishes to explore the similarity between the IP observed here and the unique packing of MRJ state of hard spheres [6]—a recently proposed concept to define an ideal amorphous solid [19]. The MRJ state can be generated by compressing a hard-sphere fluid at an infinite compression rate as described by Lubachevesky and Stillinger (LS) [5,14,20]. We reproduced the MRJ state with an average packing fraction of 0.639 in 50 compression runs by using the LS algorithm with very large compression rates. Changing the compression rate only prolongs the simulation time to reach the strictly jammed state, without affecting the stable MRJ packing fraction attainable. A different packing protocol using the Jordrey-Tory method [21] yielded the same

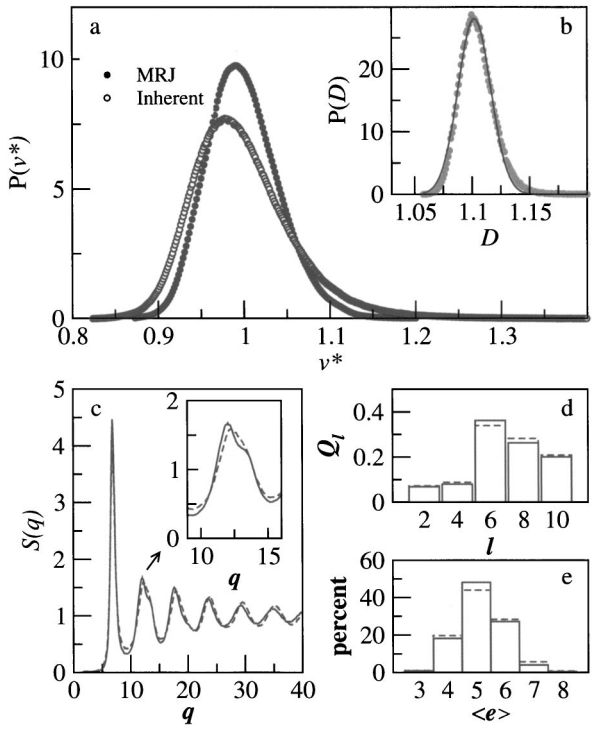

FIG. 3. (Color online) Comparison between the inherent structure of the liquid ($\rho=0.9$) and the MRJ state of hard spheres. (a) The volume distribution. (b) The probability distribution of the atomic diameter $P(D)$ showing the size dispersity in the inherent packing. The solid line is the best Gaussian fit. (c) The static structure factors, $S(q)$. (d) The local bond-orientaional parameters Q_l; (e) the percentage of average edges per face $\langle e\rangle$ of the Voronoi polyhedra; Note that fivefold symmetric bonds correspond to $\langle e\rangle$ equal to 5. Solid lines: inherent packing of the liquid; dashed lines: MRJ of hard spheres.

structure with the packing fraction of 0.639. Subsequent Voronoi construction of the as-obtained MRJ state gives the volume distribution curve in Fig. 3, which exhibits some differences from that of the IP structure. However, a more detailed geometrical analysis shown in Fig. 3 reveals that the MRJ and the IP states are closely related, in terms of their structure factors, bond-orientational order parameters, as well as bond properties.

If treating the Lennard-Jones (LJ) system as the packing of rigid spheres, we can obtain the effective diameters of the inscribed spheres from the Voronoi polyhedra. Figure 3(b) shows that this diameter has a distribution with a standard deviation of 0.015, which corresponds to ~5% of the mean. This significant size dispersity, in contrast to the delta size distribution of the spheres used to reach the MRJ state, explains the broadening of the volume distribution seen in Fig. 3(a) for the IP structure. Using this size dispersity, the real packing fraction was found to be 0.64 ± 0.01, identical to that of the MRJ state. The apparent size dispersity originates from the interatomic potentials used in the MD simulations. A harder interatomic potential results in a narrower size distribution, and vice versa, and is expected as it helps to relieve the strains and stabilize the disclination lines, thus lowering the overall free energy in relaxation. As such, the IP geometry is not reached by simply mechanically jamming a single-sized or polydispersed hard-sphere ensemble.

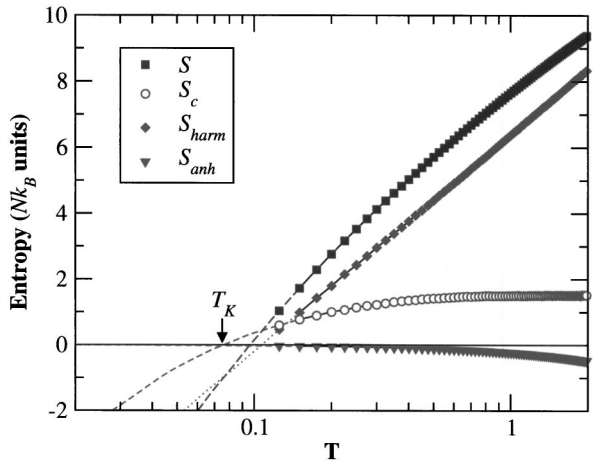

FIG. 4. (Color online) Evaluation of the (intensive) configurational entropy of the inherent structures in Fig. 1. The dashed line for the total entropy of the liquid was extrapolated according to $S-1.5Nk_B\ln T=11.0658-3.4066T^{-0.34}$. T_K denotes the hypothetical Kauzmann temperature where S_{conf} of the liquid vanishes.

The IP and MRJ states are mutually accessible. For instance, the MRJ state can be relaxed using real interatomic potentials (LJ in our case) by minimizing the potential energy of the system and finding a local minimum. Subsequent Voronoi tessellation shows that the geometry of the relaxed MRJ state is exactly the same as that of the IP obtained using the same specific potential. This indicates that the IP of the liquid is intrinsically connected with the MRJ state.

The packing complexity can be represented by its packing entropy that can be deduced from the size and shape distributions [22,23]. We estimate the configurational entropy using the Stillinger-Webber decomposition method [3,24,25],

$$S_{conf}(T,V_0)=S(T,V_0)-S_{harm}(T,V_0)-S_{anh}(T,V_0),$$

at each T. Here, S is the total liquid entropy, and S_{harm} and S_{anh} are the entropies due to the harmonic and anharmonic vibrations, respectively. To calculate the liquid entropy we perform a thermodynamic integration first along the $T=10$ isotherm, from infinite volume down to V_0, followed by a T integration of the specific heat at fixed volume V_0 according to

$$S=S_0+\int_{T_0}^{T}\frac{1}{T}\left(\frac{\partial E(T)}{\partial T'}\right)dT'.$$

By incorporating the kinetic contribution, we obtain an analytical expression which can be extrapolated to lower temperatures. S_{harm} is given by

$$S_{harm}=k_B(3N-3)\left[1-\ln\left(\frac{h\bar{\nu}}{k_BT}\right)\right],$$

where N is the number of atoms, k_B Boltzmann's constant, h Planck's constant, and ν is the calculated geometric mean value of the vibrational normal-mode frequencies

$\overline{\nu}=\Pi_{i=1}^{3N-3}(\nu_i)^{1/3N-3}$. To obtain S_{anh}, we first evaluate $E_{anh}=E(T)-E_{\mathrm{IS}}(T)-Nk_BT/2$, and fit E_{anh} with a polynomial starting from the quadratic term. Consequently, S_{anh} can be estimated by thermodynamic integration along the isochoric path between $T=0$ and the desired T.

The result given in Fig. 4 shows that the S_{conf} remains constant for all high-T equilibrium liquids. Interestingly, the IP is a structure with the maximized configurational entropy, $S_{conf}=1.5\ Nk_B$, larger than the packing entropy of hard spheres, $S_{conf}=1.0\ Nk_B$ [26]. The excess entropy S_{ex} can be attributed to the contributions from the size dispersity resulting from the application of real potentials at the given system volume. Thus, for the IP structure, $S_{conf}=S_{MRJ}+S_{ex}$, where S_{MRJ} stands for the packing entropy of the MRJ state of hard spheres. This indicates that the latter is actually the unique state with the maximum packing entropy before relaxation.

Upon supercooling to the Kauzmann temperature, calculated to be $T_K=0.075$, S_{conf} decreases to that of the corresponding crystal, resulting in an ideal glass. This low entropy state is the opposite of the IP state. Any real amorphous matter should have S_{conf} (and corresponding structural disorder) in the range bounded by these two idealized solids, i.e., the ideal glass and the ideal amorphous solid.

The inherent packing structure of the liquid can be utilized as the reference state for theoretical calculations in lieu of other approximations. In the density functional theory, an underlying structure for the liquid has long been suggested, e.g., the Bernal model generated using the Bennett algorithm [28] was taken as the reference structure in the simulation of hard-sphere liquids [27]. Our work provides the concrete evidence that a statistically unique underlying structure can indeed be defined, as well as a methodology to reach it. Due to its mechanical stability and maximum randomness, the ideal amorphous state is also useful for studies on the thermodynamics, physical properties, and deformation mechanisms of amorphous matter, including complex systems exhibiting liquid-liquid polyamorphic transitions [29].

This work was supported by the U.S. Department of Energy, Grant No. DE-FG02-03ER46056.

[1] P. M. Chaikin and T. C. Lubensky, *Principles of Condensed Matter Physics* (Cambridge University Press, Cambridge, England, 1995).
[2] F. Spaepen, Nature (London) **408**, 781 (2000).
[3] F. H. Stillinger and T. A. Weber, Phys. Rev. A **25**, 978 (1982); Science **225**, 983 (1984).
[4] J. D. Bernal, Nature (London) **185**, 68 (1960); Proc. R. Soc. London, Ser. A **280**, 299 (1964).
[5] N. H. March and M. P. Tosi, *Introduction to Liquid State Physics* (World Scientific, Singapore, 2002).
[6] S. Torquato, T. M. Truskett, and P. G. Debenedetti, Phys. Rev. Lett. **84**, 2064 (2000).
[7] D. Frenkel and B. Smit, *Understanding Molecular Simulation: From Algorithms to Applications* (Academic Press, Inc., New York, 1996).
[8] S. D. Stoddard and J. Ford, Phys. Rev. A **8**, 1504 (1973).
[9] S. Sastry, P. G. Debenedetti, and F. H. Stillinger, Nature (London) **393**, 554 (1998); S. Sastry, *ibid.* **409**, 164 (2001).
[10] P. J. Steinhardt, D. R. Nelson, and M. Ronchetti, Phys. Rev. B **28**, 784 (1983).
[11] H. Jonsson and H. C. Andersen, Phys. Rev. Lett. **60**, 2295 (1988).
[12] J. H. He *et al.*, Phys. Rev. Lett. **86**, 2826 (2001).
[13] J. R. Errington and P. G. Debenedetti, Nature (London) **409**, 318 (2001).
[14] A. R. Kansal, S. Torquato, and F. H. Stillinger, Phys. Rev. E **66**, 041109 (2002).
[15] J. R. Errington, P. G. Debenedetti, and S. Torquato, J. Chem. Phys. **118**, 2256 (2003).
[16] H. Tanaka, J. Chem. Phys. **111**, 3163 (1999).
[17] J. L. Finney, Proc. R. Soc. London, Ser. A **319**, 495 (1970); G. F. Voronoi, J. Reine Angew. Math. **134**, 198 (1908).
[18] F. W. Starr *et al.*, Phys. Rev. Lett. **89**, 125501 (2002).
[19] Z. H. Stachurski, Phys. Rev. Lett. **90**, 155502 (2003).
[20] B. D. Lubachevsky and F. H. Stillinger, J. Stat. Phys. **60**, 561 (1990).
[21] W. S. Jodrey and E. M. Tory, Phys. Rev. A **32**, 2347 (1985).
[22] S. F. Edwards and D. V. Grinev, Adv. Phys. **51**, 1669 (2002).
[23] C. E. Shannon and W. Weaver, *The Mathematical Theory of Information* (University of Illinois Press, Urbana, 1959).
[24] I. Saika-Voivod, P. H. Poole, and F. Sciortino, Nature (London) **412**, 514 (2001).
[25] F. Sciortino, W. Kob, and P. Tartaglia, Phys. Rev. Lett. **83**, 3214 (1999).
[26] A. Bonissent, J. L. Finney, and B. Mutaftschieve, Philos. Mag. B **42**, 233 (1980), and references therein.
[27] C. Kaur and S. P. Das, Phys. Rev. Lett. **86**, 2062 (2001).
[28] C. H. Bennett, J. Appl. Phys. **43**, 2727 (1972).
[29] C. A. Angell, Science **267**, 1924 (1995).
[30] The thermodynamic melting temperature T_{th} was determined using the thermodynamic integration method. At T_{th}, the Helmhotz free energy of the LJ crystal and that of the corresponding liquid are equal.